https://doi.org/10.5194/hess-2019-556
Preprint. Discussion started: 12 November 2019

Hydrology and Earth System Sciences
Discussions

Should altitudinal gradients of temperature and precipitation inputs be inferred from key parameters in snow-hydrological models?

Denis Ruelland

CNRS, HydroSciences Montpellier, University of Montpellier, Place E. Bataillon, 34395 Montpellier Cedex 5, France

Correspondence to: denis.ruelland@umontpellier.fr

Abstract. This paper evaluates whether snow-covered area and streamflow measurements can help assess altitudinal gradients of temperature and precipitation in data-scarce mountainous areas more realistically than using the usual interpolation procedures. An extensive dataset covering 20 Alpine catchments is used to investigate this issue. Elevation dependency in the meteorological fields is accounted for using two approaches: (i) by estimating the local and time-varying altitudinal gradients from the available gauge network based on deterministic and geostatistical interpolation methods with an external drift; and (ii) by calibrating the local gradients using an inverse snow-hydrological modelling framework. For the second approach, a simple 2-parameter model is proposed to target the temperature/precipitation-elevation relationship and to regionalise air temperature and precipitation from the sparse meteorological network. The coherence of the two approaches is evaluated by benchmarking several hydrological variables (snow-covered area, streamflow and water balance) computed with snow-hydrological models fed with the interpolated datasets and checked against available measurements. Results show that accounting for elevation dependency from scattered observations when interpolating air temperature and precipitation cannot provide sufficiently accurate inputs for models. The lack of high-elevation stations seriously limits correct estimation of lapse rates of temperature and precipitation, which, in turn, affects the performance of the snow-hydrological simulations due to imprecise estimates of temperature and precipitation volumes. Instead, retrieving the local altitudinal gradients using an inverse approach enables increased accuracy in the simulation of snow cover and discharge dynamics, while limiting problems of over-calibration and equifinality.

1. INTRODUCTION

1.1. Providing accurate meteorological inputs in mountainous regions

Regionalising air temperature and precipitation is a critical step in producing accurate areal inputs for hydrological models in high altitude catchments. The ability to correctly reproduce areal precipitation is vital to avoid the failure of hydrological models, which are sensitive to input volumes at the catchment scale (e.g. Oudin et al., 2006; Nicótina et al., 2008). Accurate temperature fields are also particularly important in mountainous regions because temperature is the main driver for snow/rain partition and snowmelt, and consequently influences seasonal discharge (e.g. Hublart et al., 2015; 2016).

However, in areas with complex topography, the characteristic spatial scales of temperature and precipitation estimates are typically poorly captured, notably when the network of measurements used is sparsed. Gridded datasets obtained by interpolating measurements taken at meteorological stations are thus affected by inaccuracies, which are spatially and temporally variable and difficult to quantify (Haylock et al., 2008; Isotta et al., 2015). Measurement errors depend on local conditions and increase with terrain elevation, as the operational conditions become more extreme (Frei and Schär, 1998). In the case of precipitation, a well-known problem arises from the systematic errors associated with precipitation under-catch during snowfall (Strasser et al., 2008), especially in windy conditions (Sevruk, 2005). In addition, temperature and precipitation are under-sampled at high elevations, because meteorological stations are mainly located at low elevations for logistical reasons (Hofstra et al., 2010). This makes it difficult to derive the local and seasonal relationship between

https://doi.org/10.5194/hess-2019-556
Preprint. Discussion started: 12 November 2019

Hydrology and Earth System Sciences
Discussions

meteorological observations and topography, even though this is indispensable for accurate spatial temperature and precipitation estimates (Masson and Frei, 2014). Indeed, atmospheric uplift caused by relief tends to increase precipitation with elevation through the so-called orographic effect (Barry and Chorley, 1987). Nevertheless, precipitation accumulation trends can show considerable scatter with altitude depending on the region's exposure to wind and synoptic situations (Sevruk, 1997). The relationship between temperature and elevation is generally more obvious. The rate at which air cools with a change in elevation ranges from about -0.98 °C (100 m)$^{-1}$ for dry air (i.e., the dry-air adiabatic lapse rate) to about -0.4 °C (100 m)$^{-1}$ (i.e., the saturated adiabatic lapse rate; Dodson and Marks, 1997). Average temperature gradients of -0.60 ° (Dodson and Marks, 1997) or -0.65 °C (100 m)$^{-1}$ (Barry and Chorley, 1987) are often used when high precision is not required. However, such average values are known to be rough approximations which are not suitable for more precise studies (see e.g. Douguédroit and De Saintignon, 1984). Notably they mask significant variations in different meteorological conditions and in different seasons. For instance, temperature lapse rates are generally lower in winter than in summer, as shown by Rolland (2003) for Alpine regions.

1.2. Schemes for spatial interpolation of air temperature or precipitation

The mapping of air temperature and precipitation using discrete observations based on gauge networks has been extensively studied. Readers can refer to, for instance, Ly et al. (2013) for a review on the different deterministic and geostatistical methods designed for operational hydrology and hydrological modelling at the catchment scale.

Schemes for spatial interpolation of meteorological variables vary in three ways (Stahl et al., 2006): (1) the model used to characterise the spatial variation of the variable of interest, (2) the method used to choose the surrounding points (number or distance, angular position relative to the prediction point) and (3) the approach used to adjust for elevation. The simplest approach is to choose the nearest station and adjust for elevation according to an assumed lapse rate. However, this method is fairly crude and ignores fine-scale spatial variations. Where more than one station is used in the prediction, a model is required to determine how to interpolate from them. Interpolation weights have been estimated using approaches including inverse distance weighting (IDW) (e.g. Dodson and Marks, 1997; Shen et al., 2001; Frei, 2014) and geostatistical methods based on kriging (e.g. Garen and Marks, 2005; Spadavecchia and Williams, 2009). Kriging relies on statistical models involving autocorrelation, which refers to the statistical relationships between measured points. Ordinary kriging (OKR) is well-known among kriging algorithms (see e.g. Goovaerts, 1997 for a detailed presentation of these algorithms). Different methods have been developed to deal with the statistical relationship between temperature/precipitation and elevation like regression analysis (Drogue et al., 2002), or more elaborate geostatistical techniques including simple kriging with local means, kriging with external drift (KED) and co-kriging (CKR): see Goovaerts (2000) for a comparison of these approaches. Among these techniques, KED has been widely used to generate temperature and precipitation maps. For instance, Masson and Frei (2014) showed that KED led to much smaller interpolation errors than linear regressions in the Alps. This was achieved with a single predictor (local topographic height), whereas the incorporation of more extended predictor sets (slope, circulation-type dependence of the relationship, inclusion of a wind-aligned predictor) enabled only marginal improvement. For daily precipitation, interpolation accuracy improved considerably with KED and the use of a simple digital elevation compared to OKR (i.e., with no predictor). These results confirm that accounting for topography is important for spatial interpolation of daily precipitation in high-mountain regions. Conversely, other authors showed that, even though taking topography into account was indispensable for temperature reconstruction whatever the temporal resolution, it was less clear for daily precipitation. For example, Ly et al. (2011) reported no improvement in precipitation estimated at a daily time scale if topographical information was taken into account with KED and CKR, compared to simpler methods such as ORK and IDW. In a recent and very complete comparative study, Berndt and Haberlandt (2018) analysed the influence of temporal resolution and network density on the spatial interpolation of climate variables. They showed that KED using elevation

https://doi.org/10.5194/hess-2019-556
Preprint. Discussion started: 12 November 2019

performed significantly better than ORK for temperature data at all temporal resolutions and station densities. For precipitation, using elevation as additional information in KED improved the interpolation performance at the annual time scale, but not at the daily time scale.

Theoretically, KED can account for local differences in topographic influence in different seasons and synoptic situations. Indeed, the regression coefficients computed between the primary variable (temperature or precipitation) and the secondary variable (elevation) are implicitly estimated through the kriging system within each search neighbourhood (Goovaerts, 2000). The relation between variables is thus assessed locally, meaning changes in correlation across the study area can be taken into account. However, as suggested by Stahl et al. (2006) concerning temperature and by Ly et al. (2011) concerning precipitation, care should be taken in applying KED when interpolating daily variables with very few neighbouring sample points. Indeed, methods that compute local lapse rates from the surrounding control points can perform poorly in regions with insufficient high-elevation data, due to inaccurate estimation of local lapse rates.

1.3. Placing meteorological fields in a hydrological perspective

A subject that requires further investigation is which methods that produce daily temperature and precipitation fields can provide the best snow cover and streamflow simulations. The usual cross validation for the inter-comparison of interpolation methods is limited, especially in ungauged areas, like the highest parts of mountainous areas. As stressed by Gottardi et al. (2012), a method can perform well in interpolation (at the ground network altitudes) but poorly in extrapolation (higher). This is because the observed set is not representative of the entire feature space. As a result, estimations at high elevations are difficult to check due to the lack of meteorological data. To go further, the use of other data like streamflow measurements may be a good alternative way to validate temperature and precipitation estimations at high-elevation sites.

To date, few studies have compared the performance of different interpolation methods evaluated by hydrological modelling in mountainous areas. Among the few that have, Tobin et al. (2011) showed that kriging (and more specifically KED) can be used effectively to estimate temperature and precipitation fields in complex alpine topography during flood events. Their comparative analyses of the different interpolation techniques suggested that geostatistical methods performed better than IDW. In particular, with elevation as auxiliary information, KED gave the overall best validation statistics for the set of events under study. However, it can be hypothesised that, in many mountainous areas, gauge observations do not include sufficient information to accurately account for the elevation dependency of air temperature and precipitation using interpolation techniques, which are thus limited to providing accurate inputs for snow-hydrological models. On the other hand, numerous calibration parameters controlling snow accumulation (the temperature threshold between the solid and liquid phase, temperature range of phase separation, snowfall gauge under-catch factor) and melt (temperature threshold for snowmelt, degree-day melt factor, snowpack thermal state, etc.) have been introduced in most of the snow accounting routines (SAR) used in operational hydrology: see e.g. HBV (Bergström, 1975), MOHYSE (Fortin and Turcotte, 2007), CEMANEIGE (Valéry et al., 2014), MORDOR (Garavaglia et al., 2017). The aim of using these parameters is to adapt to local snow processes, but they could be used primarily to compensate for errors in the input data without satisfactorily achieving it.

1.4. Inverting the hydrological cycle

In contrast, inverting the hydrological cycle with snow-hydrological models may help identify the dependency of the areal inputs on elevation more realistically and enable more accurate snow-hydrological simulations, while simultaneously limiting the number of free parameters. The idea is not completely new and was notably introduced by Valéry et al. (2009) in an attempt to use streamflow measurements to improve knowledge of yearly precipitation in data-sparse mountainous regions. Their results suggested that it was possible to unambiguously identify the altitudinal precipitation gradients from streamflow at a yearly time scale. In another paper, Valéry et al. (2010) proposed regionalisation of daily air temperature and

https://doi.org/10.5194/hess-2019-556
Preprint. Discussion started: 12 November 2019

precipitation to better estimate inputs over high-altitude catchments as regards to the water balance. In their conclusion, the authors claimed that their regionalisation approach also significantly improved the performance of a rainfall-runoff model at a daily time scale. However, the lapse rates in the temperature and precipitation inputs were estimated from gauge observations at the regional scale based on a leave-one-out procedure. This leaves room for potential improvement by locally inferring the lapse rates based on inverse modelling applied at the catchment scale. Improvement is also to be expected from the use of auxiliary observations such as remotely-sensed snow cover data to calibrate and validate models in addition to the runoff measurements, which can help better assess the reliability of the modelled snow processes (see e.g. Parajka and Blöschl, 2008; Thirel et al., 2013). Moreover, other authors (Franz and Karsten, 2013; He et al., 2014) showed that adding snow data information to the calibration procedure enabled the identification of more robust snow parameter sets by making the snow models less dependent on the rainfall-runoff model with which they are coupled. Using both streamflow and snow-cover observations in an inverse modelling approach could thus provide further insights into the most relevant snow parameters, while improving our knowledge of the altitudinal temperature and precipitation gradients in data-sparse mountainous regions.

1.5. Objectives

Based on the above issues, this paper investigates whether altitudinal gradients should be inferred from available gauge information when interpolating air temperature and precipitation, or from key-parameters of snow-hydrological models in mountainous areas. To address this question, we use a large dataset of mountainous, snow-affected catchments in the French Alps and we propose a framework to assess the hydrological coherence of gridded datasets and for inferring orographic gradients based on snow-hydrological observations. The rest of the paper is organised as follows. Section 2 describes the study region, the data and their pre-processing. Section 3 provides a brief description of the interpolation procedures tested. Section 4 presents the model assessment methodology. The results are presented and discussed in Section 5, and the main findings, recommendations and future outlooks are summarised in Section 6.

2. STUDY AREA AND DATASET

2.1. Meteorological data

The study was carried out in the French Alps whose altitudes range from 3 to nearly 4800 m a.s.l. (Fig. 1). A dataset of 78 temperature gauges and 148 precipitation gauges was gathered from the RADOME (*Réseau Automatisé d'Observations Météorologiques Etendues*) database of Météo-France (https://publitheque.meteo.fr) for six administrative departments (*Alpes-de-Haute-Provence*, *Hautes-Alpes*, *Alpes-Maritimes*, *Isère*, *Savoie* and *Haute-Savoie*). The extracted series are the mean daily air temperature and the daily liquid equivalent water depth of total precipitation for each station over an 18-year period from the 1st of September 1998 to the 31st of August 2016. These gauges were selected because their series present no missing data from the 1st September 2000 to the 31st of August 2016, thus allowing a coherent and stable signal to be represented over the 16-year period of analysis. The corresponding gauge density is ~3 stations per 1000 km² for temperature and ~5 stations per 1000 km² for precipitation, which is close to the recommended minimum density for mountainous areas (~4 stations per 1000 km², WMO, 2008). Although the spatial distribution of the available meteorological stations is reasonably balanced, high altitudes (above 2000 m a.s.l.), which represent approximately 20% of the study area, remain under-represented, as temperature and precipitation gauges are mainly located at low and mid elevations: between 235 and 2105 m for temperature, and between 235 and 2006 m for precipitation.

https://doi.org/10.5194/hess-2019-556
Preprint. Discussion started: 12 November 2019

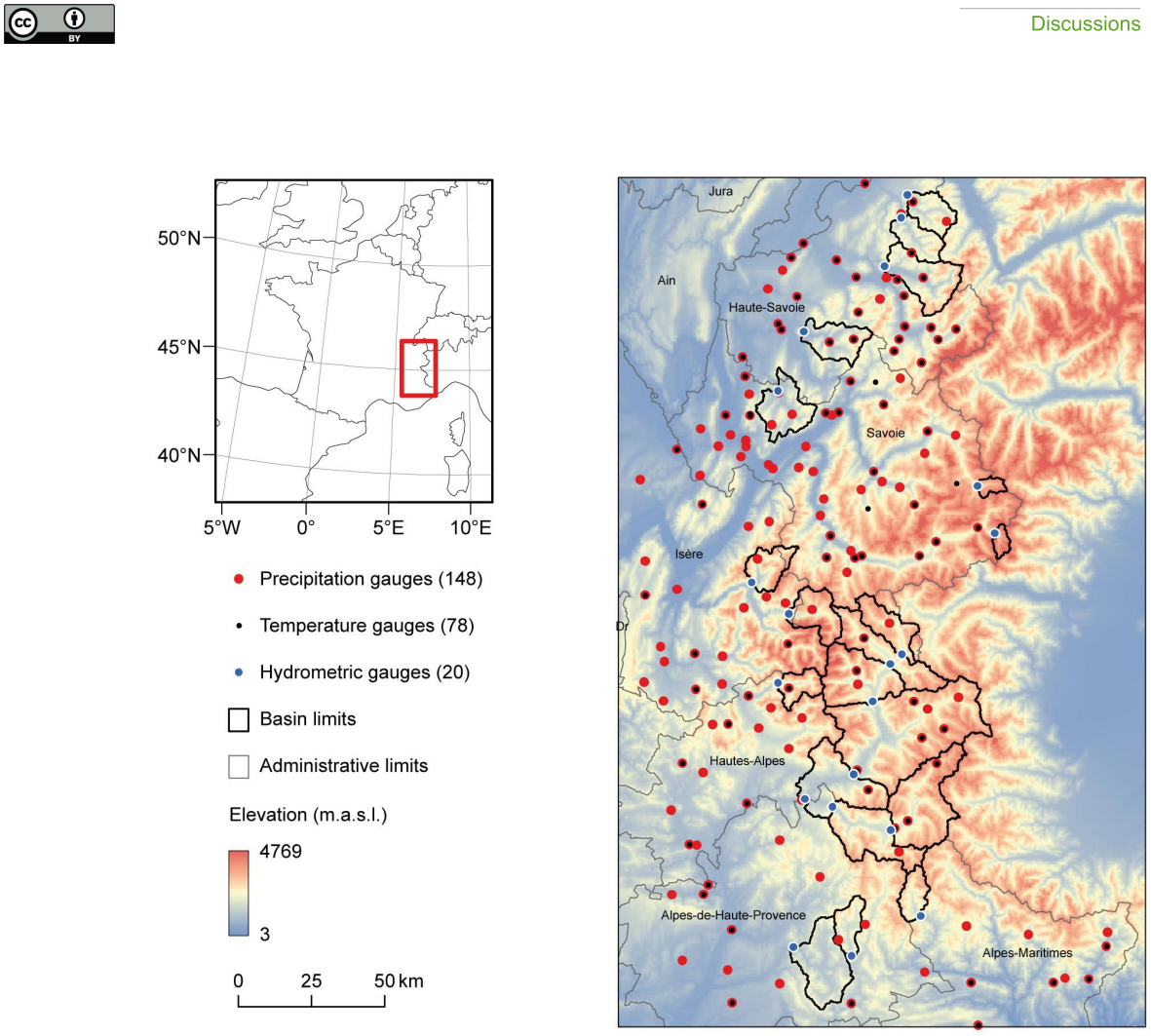

Fig. 1 Location of the selected precipitation, temperature and streamflow stations in the French Alps. Elevations are from a SRTM digital elevation model which was resampled to a grid with 0.5x 0.5 km cells.

2.2. Streamflow data

In order to avoid case-specific results, an extensive dataset of 20 catchments was gathered from the French hydrological database (www.hydro.eaufrance.fr) over the study area (Fig. 1 and Table 1). The catchments were selected based on the following criteria: (i) their streamflow regime is considered to be natural since they are located upstream from any major hydraulic installations, such as dams and water transfers; (ii) their streamflow regime is moderately to strongly affected by snow (i.e. between 10% and 70% of their total precipitation falls in solid form); and (iii) their streamflow series present good quality measurements according to the hydrological reports, with less than 10% daily missing values for the period 2000–2016.

2.3. Snow cover data

MOD10A1 (Terra) and MYD10A1 (Aqua) snow products version 5 were downloaded from the National Snow and Ice Data Center for the period 24 February 2000–1 January 2017. This corresponds to 6157 dates among which 98.8% are available for MOD10A1 and 85.8% for MYD10A1 since Aqua was launched in May 2002 and became operational in July 2002. These snow products are derived from a Normalised Difference Snow Index (NDSI) calculated from the near-infrared and green wavelengths, and for which a threshold was defined for the detection of snow (Hall et al., 2006, 2007). Cloud cover represents a significant limit for these products, which are generated from instruments operating in the visible-near-infrared

https://doi.org/10.5194/hess-2019-556
Preprint. Discussion started: 12 November 2019

Hydrology and Earth System Sciences
Discussions

wavelengths. As a result, the grid cells were gap filled to produce daily cloud-free snow cover maps of the study area. The different classes in the original products were first merged into three classes: no-snow (no snow or lake), snow (snow or lake ice), no-data (clouds, missing data, no decision, or saturated detector). The missing values were then filled according to a gap-filling algorithm described in Gascoin et al. (2015). The algorithm works in three sequential steps: (i) Aqua/Terra combination; (ii) temporal deduction by sliding the time filter up to 9 days; (iii) spatial deduction by elevation and neighbourhood filter to fill the remaining gaps. The resulting database consists of 5844 binary (snow/no-snow) maps at 500 m spatial resolution for the period 2000–2016 (16 hydrological years, from the 1st of September 2000 to the 31st of August 2016).

Table 1 Streamflow gauging stations and main catchment characteristics. The fraction of precipitation falling as snow (Snow) was estimated by hydrological modelling.

#	Station	River	Area	Elevations (m a.s.l.)			Snow	Operator
			(km²)	Min	Mean	Max	%	
1	Barcelonnette [Abattoir]	Ubaye	549	1132	2214	3308	48	DREAL
2	Lauzet-Ubaye [Roche Rousse]	Ubaye	946	790	2083	3308	41	EDF
3	Beynes [Chabrières]	Asse	375	605	1137	2273	14	EDF
4	Saint-André-Les-Alpes [Mourefrey]	Issole	137	931	1502	2392	22	DREAL
5	Villar-Lourbière	Séveraisse	133	1023	2172	3623	48	DREAL
6	Val-des-Prés	Durance	207	1360	2221	3059	53	DREAL
7	Briançon	Durance	548	1187	2187	3572	51	EDF
8	Argentière-la-Bessée	Durance	984	950	2178	4017	54	DREAL
9	Embrun [La Clapière]	Durance	2170	787	2109	4017	49	EDF
10	Espinasses [Serre-Ponçon]	Durance	3580	652	2029	4017	49	EDF
11	Villeneuve-d'Entraunes [Pont d'Enaux]	Var	132	926	1902	2862	35	DREAL
12	Val-d'Isère	Isère	46	1831	2659	3538	64	EDF
13	Bessans [Avérole]	Avérole	45	1950	2871	3670	71	EDF
14	Taninges [Pressy]	Giffre	325	615	1507	3044	34	EDF
15	Vacheresse	Dranse d'Abondance	175	720	1443	2405	29	DREAL
16	La Baume [Pont de Couvaloup]	Dranse de Morzine	170	690	1437	2434	27	DREAL
17	Dingy-Saint-Clair	Fier	223	514	1244	2545	20	DREAL
18	Allèves [La Charniaz]	Chéran	249	575	1171	2157	23	DREAL
19	Mizoën [Chambon amont]	Romanche	220	1057	2396	3846	53	EDF
20	Allemond [La Pernière]	L'Eau Dolle	172	713	1964	3430	47	EDF

3. INTERPOLATION PROCEDURES

This section briefly presents the different spatial estimators used in the present study. The interpolation methods analysed include inverse distance weighted (IDW), ordinary kriging (ORK), kriging with external drift (KED) and IDW with external drift (IED). Interest readers can refer to Goovaerts (2000) for a detailed presentation of the different kriging algorithms, and to Diggle and Ribeiro (2007) for their implementation in the public domain in the *GeoPackage* in *R*.

3.1. Spatial interpolation methods

3.1.1. Inverse distance weighting

Let us consider the problem of estimating the given variable z at an unsampled location u using only surrounding observation data. Let $\{z(u_\alpha), \alpha = 1, \ldots, n\}$ be the set of data measured at n surrounding locations u_α. The inverse distance weighting (IDW) method estimated z as a linear combination of $n(u)$ surrounding observations with the weights being inversely proportional to the square ω distance between observations and u:

$$Z_{\mathrm{IDW}}(u) = \frac{1}{\sum_{\alpha=1}^{n(u)} \lambda_\alpha(u)} \sum_{\alpha=1}^{n(u)} \lambda_\alpha(u) z(u_\alpha) \quad \text{with} \quad \lambda_\alpha(u) = \frac{1}{|u - u_\alpha|^\omega} \tag{1}$$

https://doi.org/10.5194/hess-2019-556
Preprint. Discussion started: 12 November 2019

Hydrology and Earth System Sciences
Discussions

The basic idea behind the weighting scheme is that observations that are close to each other on the ground tend to be more alike than those located further apart, hence observations closer to *u* should receive a larger weight.

3.1.2. Ordinary kriging

Instead of Euclidian distance, geostatistics uses the semivariogram as a measure of dissimilarity between observations. The experimental semivariogram is computed as half the average squared difference between the components of data pairs:

$$\hat{\gamma}(h) = \frac{1}{2N(h)} \sum_{\propto=1}^{N(h)} [z(u_\alpha) - z(u_\alpha + h)]^2 \quad (2)$$

where *N(h)* is the number of pairs of data locations a vector *h* apart. The hypotheses of spatial variability were here homogeneity and an isotropic spatial pattern due to the lack of sufficient sampled points, and hence identical variability in all directions.

Kriging is a generalized least-squares regression technique that makes it possible to account for the spatial dependence between observations, as revealed by the semivariogram, in spatial prediction. Like the inverse distance weighting method, ordinary kriging (ORK) estimates the unknown variable *z* at the unsampled location *u* as a linear combination of neighbouring observations:

$$Z_{\mathrm{ORK}}(u) = \sum_{\alpha=1}^{n(u)} \lambda_\alpha^{ORK}(u) z(u_\alpha) \quad \text{with} \quad \sum_{\alpha=1}^{n(u)} \lambda_\alpha^{ORK}(u) = 1 \quad (3)$$

The ordinary kriging weights $\lambda_\alpha^{ORK}(u)$ are determined such as to minimise the estimation variance $Var\{Z_{\mathrm{ORK}}(u) - \mathrm{z(u)}\}$,while ensuring the unbiasedness of the estimator $E\{Z_{\mathrm{ORK}}(u) - \mathrm{z(u)}\} = 0$. These weights are obtained by solving a system of linear equations known as the ordinary kriging system:

$$\begin{cases} \sum_{\beta=1}^{n(u)} \lambda_\beta(u)\gamma(u_\alpha - u_\beta) - \mu(u) = \gamma(u_\alpha - u) & \alpha = 1, \ldots, n(u) \\ \sum_{\beta=1}^{n(u)} \lambda_\beta(u) = 1 \end{cases} \quad (4)$$

where $\mu(u)$ are Lagrange parameters accounting for the constraints on the weights. The only information required by the kriging system (4) are semivariogram values for different lags, and these are readily derived once a semivariogram model has been fitted to experimental values. In this study, we dealt with the fitting of the semivariogram using two existing theoretical models, as presented below:

- Exponential model

$$\gamma(h;\theta) \begin{cases} 0, & \mathrm{h} = 0, \\ \theta_0 + \theta_1[1 - \exp(-3(\|h\|/\theta_2], & \mathrm{h} \neq 0, \end{cases} \quad (5)$$

https://doi.org/10.5194/hess-2019-556
Preprint. Discussion started: 12 November 2019

Hydrology and Earth System Sciences
Discussions

for $\theta_0 \geq 0,\ \theta_1 \geq 0\ and\ \theta_2 \geq 0$.

- Spherical model

$$\gamma(h;\theta)\begin{cases}0, & \mathrm{h} = 0,\\ \theta_0 + \theta_1\left(\frac{3\|h\|}{2\theta_2} - \frac{1}{2}\left(\frac{\|h\|}{\theta_2}\right)^3\right), & 0 < \|h\| \leq \theta_2,\\ \theta_0 + \theta_1, & \mathrm{h} > \theta_2,\end{cases} \quad (6)$$

for $\theta_0 \geq 0,\ \theta_1 \geq 0\ and\ \theta_2 \geq 0$.

The spherical model was tested because it is the most widely used semivariogram model and is characterised by linear behaviour (Goovaerts, 2000). The exponential model was selected in addition because it is recommended in the literature for spatial analysis of temperature (Tobin et al., 2011) and precipitation (Bárdossy and Pegram, 2013; Masson and Frei, 2014) in high-mountain regions. Each of these models was combined with a nugget effect, sill and range as parameters. An automatic procedure was necessary to fit the semivariogram model to experimental values over the study period (1998–2016). The models were fitted using regression such that the weighted sum of squares of differences between the experimental and model semivariogram is minimum (see Goovaerts, 2000).

3.2. Accounting for elevation dependency

3.2.1. Kriging with external drift

Kriging with an external drift (KED) predicts sparse variables which are poorly correlated in space by considering that there is a local trend within the neighbourhood; primary data is assumed to have a linear relation with auxiliary information exhaustively sampled over the study area (Ahmed and de Marsily, 1997). KED thus uses secondary information (such as elevation) to derive the local mean of the primary attribute *z* and then performs kriging on the corresponding residuals:

$$Z_{\mathrm{KED}}(u) - m_{\mathrm{KED}}(u) = \sum_{\alpha=1}^{n(u)} \lambda_\alpha^{KED}(u)[z(u_\alpha) - m_{\mathrm{KED}}(u_\alpha)] \quad (7)$$

with $m_{\mathrm{KED}}(u) = a_0(u) + a_1(u)y(u)$

where $y(u)$ are elevation data available at all estimation points, a_0 and a_1 are two regression coefficients estimated from the set of collocated variable of interest and elevation data $\{z(u_\alpha), y(u_\alpha), \alpha = 1, \ldots, n\}$ using a simple linear relation.

The KED procedure was applied at each time step independently and within each search neighbourhood when the time series were interpolated. The coefficients a_0 and a_1 thus varied in space and time, which makes possible to consider a variable space-time relationship between the primary variable (temperature or precipitation) and the secondary variable (elevation).

3.2.2. Inverse distance weighting with external drift (IED)

The external drift approach was also tested using the inverse distance weighting procedure to propose an original technique, which we called IDW with external drift (IED), as follows:

https://doi.org/10.5194/hess-2019-556
Preprint. Discussion started: 12 November 2019

Hydrology and Earth System Sciences
Discussions

$$Z_{\mathrm{IED}}(u) - m_{\mathrm{IED}}(u) = \frac{1}{\sum_{\alpha=1}^{n(u)} \lambda_\alpha(u)} \sum_{\alpha=1}^{n(u)} \lambda_\alpha(u)[z(u_\alpha) - m_{\mathrm{IED}}(u_\alpha)] \quad (8)$$

with $m_{\mathrm{IED}}(u) = a_0(u) + a_1(u)y(u)$

3.3. Leave-one-out procedure

The interpolation parameters ($n(u)$ and ω for IDW and IED, and $n(u)$ and theoretical models for ORK and KED) were calibrated and the interpolation performance was assessed by "leave-one-out" cross validation, which consists of the following principle: a successive estimation of all sampled locations was performed by using all other stations while always excluding the sample value at the location concerned. The spatial models were validated against RMSE (root mean square error normalized with the average of observations) for temperature and precipitation at daily, monthly and yearly time steps. For precipitation, parameters were only estimated for days with at least 1 mm mean precipitation, i.e. approximatively 41% of the daily sample, whereas parameters were calculated for all months and years since there were no locations with dry months or dry years in the dataset. Since the external drift computation and kriging weights can sometimes lead to negative precipitation amounts (Deutsch, 2006), *a posteriori* correction was performed to replace all negative-estimated precipitation values with a zero value. The following performance measures were used to compare the estimations and observations for *n* locations and *t* time steps: the RMSE, the absolute simple bias (expressed in °C or mm) and the Nash-Sutcliffe Efficiency criterion (NSE; Nash and Sutcliffe, 1970).

The elevations of the gauging stations were used when applying the KED and IED procedures for the "leave-one-out" cross validation. When interpolating temperature and precipitation exhaustively over the study area, the elevation predictors were based on the digital elevation model (DEM) of the shuffle radar topography mission (SRTM; Farr et al., 2007). SRTM originally has a resolution of about 90 m. In this study, we used the SRTM elevation model resampled to a grid with 0.5x0.5 km cells from the UTM32N coordinate reference system. This spatial resolution was judged as a good balance between computational constraints and elevation accuracy.

4. MODEL ASSESSSMENT METHODOLOGY

The way of accounting for orographic gradients in the temperature and precipitation datasets was also assessed with respect to its ability to contribute to simulations of snow covered area and streamflow at the catchment scale using the following modelling experiment.

4.1. Snow accounting routine (SAR)

The selected SAR (Fig. 2a) is a modified version of CEMANEIGE proposed by Valéry et al. (2014). The original version was modified to account for: a snowfall under-catch correction factor as used in the HBV snow routine (see Beck et al., 2016), the computation of fractional snow-covered area (FSC) from a snow water equivalent (SWE) threshold, and possible integration of temperature and precipitation altitudinal gradients.

https://doi.org/10.5194/hess-2019-556
Preprint. Discussion started: 12 November 2019

Hydrology and Earth System Sciences
Discussions
Open Access
EGU

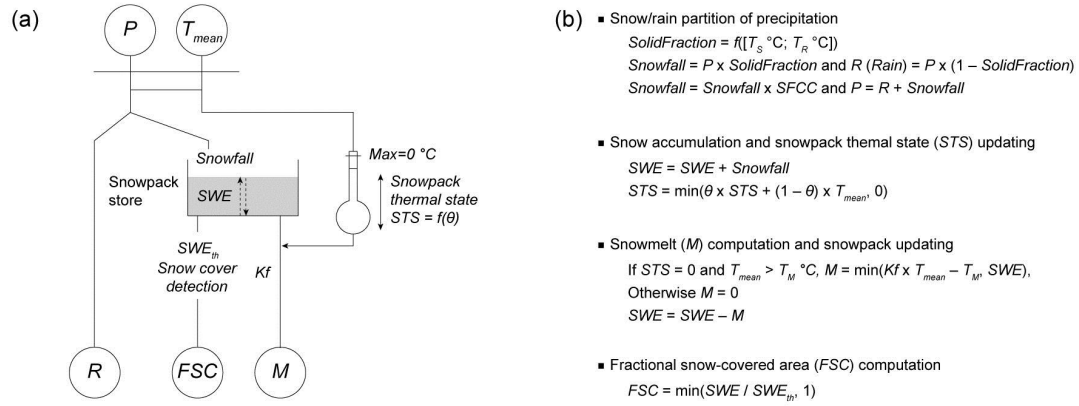

Fig. 2 Snow accounting routine: (a) conceptual scheme and (b) associated equations (modified from Valéry et al., 2014).

Depending on the objectives, the model can be run in a full distributed mode or according to elevation bands. As distributed (or semi-distributed) inputs, it requires the daily liquid equivalent water depth of total precipitation (P) and mean daily air temperature (T_{mean}). In the case of a semi-distributed application at the catchment scale, the first step is to divide the catchment into elevation zones of equal area. Mean areal inputs (P and T_{mean}) are then extracted for each elevation zone from gridded temperature and precipitation datasets. In the present study, the number of elevation zones was set at five due to computational constraints and because preliminary tests showed no significant improvement in the snow-hydrological simulations when a higher spatial resolution was used.

In each elevation band, the functions of the SAR described in Figure 2b are applied with a unique set of parameters. Internal states (snowpack represented according to snow water equivalent (*SWE*) and its thermal state *STS*) vary independently in each elevation zone according to the differences in input values. When gridded temperature and precipitation datasets interpolated without elevation dependency are used, the SAR enables forcing data for each elevation zone to be modified based on two orographic gradients (*TLR* and *PLR*) used as key parameters:

$$T_i(t) = T_i^{IDW}(t) + \left[\frac{-\left(TLR + \frac{1}{2}TLR \times Si \times CSV\right)}{100} \times (y_i - y_i^{IDW}(t))\right] \quad (9)$$

with:

$$Si \begin{cases} \sin\left(\frac{2\pi \times (d - 80.5)}{366}\right), & lat > 0 \\ -\sin\left(\frac{2\pi \times (d - 80.5)}{366}\right), & lat < 0 \end{cases}$$

$$P_i(t) = P_i^{IDW}(t) \times [1 + \tfrac{PLR}{1000} \times (y_i - y_i^{IDW}(t))] \quad (10)$$

where $T_i^{IDW}(t)$ and $P_i^{IDW}(t)$ are, respectively, the mean areal temperature and precipitation interpolated based on the IDW procedure in elevation zone i at time step t; $y_i^{IDW}(t)$ is the mean areal elevation interpolated based on the IDW procedure in elevation zone i from the available gauges at time step t; y_i is the mean areal elevation extracted from the DEM in elevation zone i; *TLR* and *PLR* are the constant temperature and precipitation lapse rates to be calibrated; *CSV* is a coefficient of seasonal variation due to solar radiation to be applied to *TLR* (when set to 0, no seasonal variation is applied); *Si* is an index

https://doi.org/10.5194/hess-2019-556
Preprint. Discussion started: 12 November 2019

Hydrology and Earth System Sciences
Discussions

of seasonal change in solar radiation accounting for daytime length and ranges from -1 on the 21st of December (winter solstice) to 1 on the 21st of June (summer solstice) in non-leap years in the Northern Hemisphere ($lat > 0$), d is the number of days since the 1st of January of the current year.

To ensure insightful comparison with the modelling experiment, the SAR was calibrated according to different modes and degrees of freedom (Table 2). In mode *M1*, elevation dependency, which was accounted for (or not) in the *T* and *P* inputs based on the interpolation procedures, was tested by calibrating five parameters (T_S, T_R, *SFCC*, θ, *Kf*) which control snow accumulation and melt. This mode is usually used to allow snow processes to be adjusted to local conditions and/or the errors in the *T* and *P* inputs. In mode *M2*, all parameters of the SAR were fixed in order to introduce two parameters (*TLR* and *PLR*) as orographic gradients. The aim of using this mode was to account for elevation dependency in the *T* and *P* inputs from constant, calibrated orographic gradients while fixing the parameters that control snow accumulation and melt. In mode *M3*, the same approach was chosen but an additional parameter (*CSV*) was associated with the *TLR* gradient in order to test the value of introducing a seasonal variation in the temperature lapse rates (see Eq. 9). In mode *M4*, elevation dependency in the *T* and *P* inputs was also accounted for based on three (*TLR*, *CSV* and *PLR*) parameters and two other parameters (θ, *Kf*) were calibrated in addition to allow for snowmelt adjustment.

In each altitudinal band, five outputs (rainfall, snowfall, snowmelt, potential evapotranspiration and fractional snow-covered area) are computed at each daily time step. Rainfall (*R*) and snowmelt (*M*) are summed to compute the total quantity of water available for production and transfer in the catchment. Potential evapotranspiration (*PE*) is computed for each altitudinal band using the temperature-based formulation proposed by Oudin et al. (2005):

$$PE_i(t) = \frac{R_e}{\lambda\rho}\frac{T_i(t)+5}{100} \quad \text{if } (T_i(t)+5) > 0; \quad else\ PE_i(t) = 0 \tag{11}$$

where R_e is the extra-terrestrial solar radiation (MJ.m^{-2}.day^{-1}) which depends on the latitude of the basin and the Julian day of the year, λ is the net latent heat flux (fixed at 2.45 MJ.kg^{-1}), ρ is the water density (set at 11.6 kg.m^{-3}) and $T_i(t)$ is the air temperature (°C) estimated in the elevation zone *i* at time step *t*.

Table 2 Parameters of the snow accounting routine and their associated fixed values or ranges tested in each modelling experiment.

			Fixed values or ranges tested			
Param.	Meaning	Unit	*M1*	*M2*	*M3*	*M4*
T_S	Temperature between the solid and liquid phase	°C	[-3; 3]	-1	-1	-1
T_R	Thermal range for the phase separation above T_S	°C	[0; 10]	4	4	4
SFCC	Snowfall gauge under-catch correction factor	-	[1; 3]	1	1	1
θ	Weighting coefficient for snowpack thermal state	-	[0; 1]	0	0	[0; 1]
T_M	Temperature threshold for snowmelt	°C	T_S + 1	0	0	0
Kf	Degree-day melt factor	mm.°C^{-1}.d^{-1}	[0; 10]	5	5	[0; 10]
SWE_{th}	Snow water equivalent threshold to compute FSC	mm	40	40	40	40
TLR	Temperature lapse rate	°C (100m)$^{-1}$	-	[0;1.5]	[0;1.5]	[0;1.5]
CSV	Coefficient of seasonal variation applied to *TLR*	-	-	0	[0; 1]	[0; 1]
PLR	Precipitation lapse rate	% (km)$^{-1}$	-	[0; 200]	[0; 200]	[0; 200]

The outputs of each band are averaged to estimate the total liquid output of the SAR and *PE* at the catchment scale in order to feed the combined hydrological models (Fig. 3).

4.2. Hydrological models

To avoid model-specific results, two well-known hydrological models (see structures in Fig. 3 and parameters in Table 3) were chosen in association with the SAR: the 4-parameter GR4J presented by Perrin et al. (2003) and a 9-parameter lumped

https://doi.org/10.5194/hess-2019-556
Preprint. Discussion started: 12 November 2019

Hydrology and Earth System Sciences
Discussions
Open Access
EGU

version of the HBV model (Bergström, 1995; Beck et al., 2016), here referred to as HBV9 to avoid confusion with the original version.

The two models were run at a daily time step and used in lumped mode with the SAR on top. The structure and the number of degrees of freedom differ between GR4J and HBV9, which should make our results more generalizable.

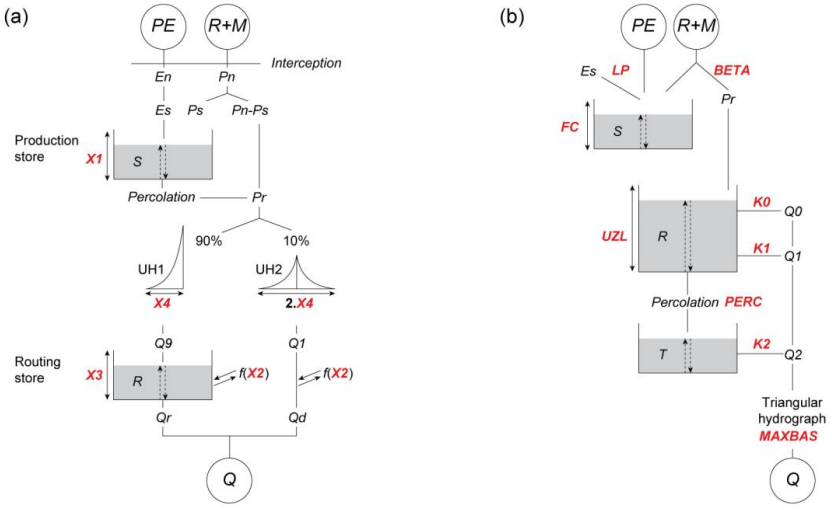

Fig. 3 Diagrams of the two hydrological models used: (a) GR4J and (b) HBV9. Calibrated parameters are in red and are further described in Table 3.

Table 3 Parameters of the hydrological models and their associated ranges tested.

Model	Parameter	Meaning	Unit	Tested range
GR4J	*X1*	Maximum capacity of the production store *S*	mm	[10; 1000]
	X2	Inter-catchment exchange coefficient	$mm.d^{-1}$	[-5; 5]
	X3	Maximum capacity of the non-linear routing store *R*	mm	[0; 500]
	X4	Unit hydrograph (UH) time base	d	[0.5; 5]
HBV9	*BETA*	Shape coefficient of recharge function	-	[0.5; 5]
	FC	Maximum water storage in the unsaturated-zone store *S*	mm	[10; 1500]
	LP	Fraction of soil moisture above which actual evapotranspiration reaches PE	-	[0.3; 1]
	K0	Additional recession coefficient of the upper groundwater store *R*	-	[0.05; 1]
	K1	Recession coefficient of the upper groundwater store *R*	-	[0.1; 0.8]
	UZL	Threshold value for extra flow from the upper zone	mm	[0; 500]
	PERC	Maximum percolation to the lower zone	$mm.d^{-1}$	[0; 6]
	K2	Recession coefficient of the lower groundwater store *T*	-	[0.01; 0.15]
	MAXBAS	Length of the equilateral triangular weighting function	-	[1 7]

4.3. Calibration and validation methods

4.3.1. General model assessment

The models (GR4J and HB9 with the SAR on top) were cross-validated using a split-sample test procedure. The simulation period (2000–2016) was split into two sub-periods alternatively used for calibration and validation. Thus two calibration and two validation tests were performed to provide results in validation on all available data. The models were run in a continuous way for the whole reference period, while only hydrological years (from the 1st of September to the 31st of August) corresponding to the calibration and validation periods were considered to compute the efficiency criteria. The 3-

https://doi.org/10.5194/hess-2019-556
Preprint. Discussion started: 12 November 2019

year period before the simulation period was used for model warm-up to limit the effect of the storage initialisation, and was not included in performance computation.

4.3.2. Optimisation algorithm and objective function

The parameters of the SAR and the hydrological model were optimised simultaneously, using the Shuffled Complex Evolution (SCE) algorithm (Duan et al., 1992). The algorithmic parameters of SCE were set to the values recommended by Duan et al. (1994) and Kuczera (1997) to reduce the risk that SCE fails in local optimal solutions. The objective function (OF) used was a multi-criteria composite function focusing simultaneously on variations in snow-covered area, streamflow dynamics and water balance at the basin scale, as follows:

$$\mathrm{OF} = 1 - \mathrm{NSE}_{\mathrm{SNOW}} + 1 - \mathrm{NSE}_{\mathrm{sqrQ}} + 1 - \mathrm{WB}$$

with:

$$\mathrm{NSE}_{\mathrm{SNOW}} = 1 - \frac{\sum_{i=1}^{N}(FSC_{sim,i} - FSC_{obs,i})^2}{\sum_{i=1}^{N}(FSC_{obs,i} - \overline{FSC_{obs}})^2} \quad (12)$$

$$\mathrm{NSE}_{\mathrm{sqrQ}} = 1 - \frac{\sum_{i=1}^{N}(\sqrt{Q_{sim,i}} - \sqrt{Q_{obs,i}})^2}{\sum_{i=1}^{N}(\sqrt{Q_{obs,i}} - \overline{\sqrt{Q_{obs}}})^2}$$

$$\mathrm{WB} = \frac{\sum_{y=1}^{M}\left[\left(Q_{sim,y} > P_y - PE_y\right) \overset{TRUE}{\longleftrightarrow} \left(Q_{sim,y} < P_y\right)\right]}{M}$$

where $FSC_{obs,i}$ and $FSC_{sim,i}$ are the observed and simulated fractional snow-covered area (FSC) at daily time step i, N is the total number of time steps, $\overline{FSC_{obs}}$ is the mean observed FSC over the test period, $Q_{obs,i}$ and $Q_{sim,i}$ are the observed and simulated streamflows at daily time step i, $\overline{\sqrt{Q_{obs}}}$ is the mean observed square root transformed flows over the test period, $Q_{sim,y}$, P_y and PE_y are the total streamflow, precipitation and potential evapotranspiration in year y and M is the total number of years in the test period.

$\mathrm{NSE}_{\mathrm{SNOW}}$ relies on the Nash-Sutcliffe Efficiency criterion. Perfect agreement between the observed and simulated values gives a score of 1, whereas a negative score represents lower reproduction quality than if the simulated values had been replaced by the mean observed values. $\mathrm{NSE}_{\mathrm{sqrQ}}$ can be considered as a multi-purpose criterion focusing on the simulated hydrograph. It puts less weight on high flows than the standard NSE on non-transformed discharge (Oudin et al., 2006). WB represents the proportion of years of the test period, which respects the water and energy balance in the Turc-Budyko non-dimensional graph proposed by Andréassian and Perrin (2012). The WB criterion evaluates if the catchment-scale annual water balance is ensured. Perfect agreement gives a WB score of 1, while 0 indicates that the water balance is not reached in any year during the test period.

4.3.3. Efficiency criteria in validation

Four criteria were used to evaluate model performance during validation. The first one was the $\mathrm{NSE}_{\mathrm{SNOW}}$ criterion. To put more emphasis on high and low flow conditions, we used the NSE on non-transformed streamflows ($\mathrm{NSE}_{\mathrm{Q}}$) that gives more weight to large errors generally associated with peak flows, and the NSE on log-transformed streamflows ($\mathrm{NSE}_{\mathrm{lnQ}}$). The

https://doi.org/10.5194/hess-2019-556
Preprint. Discussion started: 12 November 2019

absolute cumulated volume error (VE_C) was also computed to obtain information on the agreement between observed and simulated total discharge over the test periods:

$$VE_C = 1 - \frac{\left|\sum_{i=1}^{N} Q_{sim,i} - \sum_{i=1}^{N} Q_{obs,i}\right|}{\sum_{i=1}^{N} Q_{obs,i}} \quad (13)$$

A value of 1 indicates perfect agreement while values less than 1 indicate over- or underestimation of the volume.

5. RESULTS AND DISCUSSION

5.1. Cross-validation of the interpolation methods

Table 4 lists the results of cross-validation of the interpolation methods against yearly, monthly and daily series from temperature and precipitation gauges. Kriging with ORK led to an improvement over IDW only for precipitation interpolation at the yearly and monthly time scales. Considering elevation dependency with external drift (KED and IED) significantly improved the performance of the kriging and inverse-distance methods, except for precipitation estimated at the daily time scale. This shows that the correlation between precipitation and topography increases with the increasing time aggregation as already reported in other studies (e.g., Bárdossy and Pegram, 2013; Berndt and Haberlandt, 2018). Of all the methods tested, IED provided the best performance in terms of both lower RMSE and MAE, and higher NSE for each variable (temperature and precipitation) and at all temporal resolutions (yearly, monthly and daily), except for precipitation at the daily time scale for which IDW performed best.

The exponential variogram model for the ORK and KED method performed systematically better than the spherical model whatever the variable and the time scale. In contrast, the exponent ω used with the IDW and IED methods varies from 1 to 3 depending on the considered variable and time scale. The optimised number of surrounding neighbours $n(u)$ also varies depending on the method and time scale. At the daily time scale, $n(u)$ ranged from 6 when interpolating temperature with ORK to 17 when interpolating precipitation with KED and IED. Hence, 10 (17) surrounding neighbours were used to compute altitudinal gradients of temperature (precipitation) based on the daily linear regressions with KED and IED.

Figure 4 shows the annual temperature and precipitation maps obtained by interpolation daily data from the meteorological gauges with the period 2000–2016 using the IDW, ORK, KED and IED methods and their optimised parameters (Table 4). The maps of IED estimates of mean temperature and annual precipitation closely resemble the KED maps. Temperature estimates range from -9.2 °C to 16 °C with KED, and from -11.2 °C to 16.6 °C with IED. Precipitation estimates range from 630 mm to 3273 mm with KED, and from 642 mm to 3184 mm with IED. As expected, these ranges are wider than those obtained with the IDW and ORK procedures, which, unlike the KED and IED methods, do not consider either local or seasonal elevation dependency. As a result, the ranges obtained with KED and IED are probably more realistic with respect to temperature, but not necessarily with respect to precipitation, for which daily cross-validation shows that the simple IDW method provided better results. However, cross-validation was based on precipitation gauges sampled only below 2006 m a.s.l., meaning validation of the temperature and precipitation gridded datasets at higher altitudes was not possible. Another approach is thus needed to further explore whether elevation dependency should be disregarded when estimating daily precipitation (as suggested by cross-validation), and, if not, whether this dependency should be accounted for in the interpolation process or by inverting the hydrological cycle. A sensitivity analysis of snow-hydrological simulations to the orographic gradients was thus conducted.

https://doi.org/10.5194/hess-2019-556
Preprint. Discussion started: 12 November 2019

Hydrology and Earth System Sciences
Discussions
Open Access
EGU

Table 4 Cross-validation of the interpolation methods against yearly, monthly and daily series from meteorological gauges over the period 2000–2016. The best efficiency criteria for each analytical time scale and each variable of interest (temperature and precipitation) are in bold. The values of $n(u)$ and ω (for IDW and IED) and of $n(u)$ and *model* (for ORK and KED) represent the interpolation parameters, which were optimised using the leave-one-out procedure, as described in section 3.3.

		Temperature (78 gauges)				Precipitation (148 gauges)			
		Without elevation dependency		With elevation as external drift		Without elevation dependency		With elevation as external drift	
		IDW	ORK	KED	IED	IDW	ORK	KED	IED
Yearly	RMSE	1.82	1.82	0.65	**0.65**	177.05	174.27	153.75	**150.31**
	MAE	1.5 °C	1.5 °C	0.5 °C	**0.5 °C**	131.2 mm	127.8 mm	111.2 mm	**110.4 mm**
	NSE	0.452	0.455	0.931	**0.930**	0.764	0.772	0.822	**0.830**
	$n(u)$	6	6	8	10	4	15	12	12
	ω	1	-	-	2	3	-	-	3
	model	-	exponential	exponential	-	-	exponential	exponential	-
Monthly	RMSE	1.91	1.92	0.86	**0.80**	23.19	22.73	22.35	**22.20**
	MAE	1.5 °C	1.5 °C	0.6 °C	**0.6 °C**	15.5 mm	15.2 mm	14.8 mm	**14.8 mm**
	NSE	0.927	0.926	0.987	**0.987**	0.873	0.878	0.882	**0.883**
	$n(u)$	7	6	8	10	5	15	12	12
	ω	1	-	-	2	2	-	-	2
	model	-	exponential	exponential	-	-	exponential	exponential	-
Daily	RMSE	2.16	2.18	1.21	**1.20**	**4.34**	4.38	4.47	4.46
	MAE	1.7 °C	1.7 °C	0.9 °C	**0.9 °C**	**2.3 mm**	2.3 mm	2.4 mm	2.4 mm
	NSE	0.923	0.921	0.976	**0.976**	**0.833**	0.831	0.823	0.824
	$n(u)$	7	6	10	10	10	10	17	17
	ω	1	-	-	2	2	-	-	2
	model	-	exponential	exponential	-	-	exponential	exponential	-

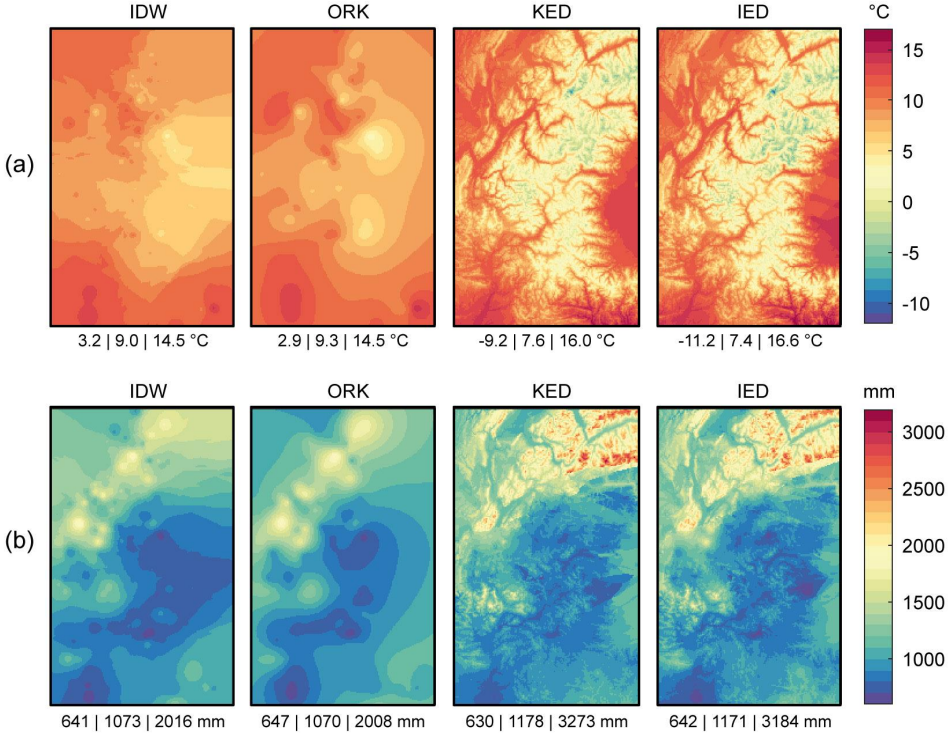

Fig. 4 Maps of mean annual temperature (°C) and total precipitation (mm per year) obtained by interpolation of (a) 78 gauges (temperature) and of (b) 148 gauges (precipitation) with daily data for the period 2000–2016 using the inverse distance weighted (IDW), ordinary kriging (ORK), kriging with external drift (KED) and IDW with external drift (IED). The numbers below each map stand respectively for minimum, mean and maximum values (expressed in °C for temperature and in mm for precipitation) in the maps.

https://doi.org/10.5194/hess-2019-556
Preprint. Discussion started: 12 November 2019

Hydrology and Earth System Sciences
Discussions

5.2. Sensitivity of the snow-hydrological simulations to the orographic gradients

For the sake of brevity, here we only present the results we obtained with the datasets interpolated with the IDW and IED procedures, since cross-validation at the daily time scale showed that they slightly outperformed the ORK and KED methods, respectively. Table 5 summarises the six tests performed to account for elevation dependency in the *T* and *P* inputs via the modelling experiment described in section 4.

Table 5 Description of the tests to account for elevation dependency in the T and P inputs via the modelling experiment described in section 4.

Mode	Test number	*T* input	*P* input	Calibrated parameters (excluding hydrological models)	Principle
M1	1	T-IDW	P-IDW	T_S, T_R, *SFCC*, θ, *Kf*	No elevation dependency in the *T* and *P* inputs, and five calibrated parameters for adjustment of snow accumulation and melt
	2	T-IED	P-IDW	T_S, T_R, *SFCC*, θ, *Kf*	Elevation dependency only in the *T* input based on the IED interpolation procedure, and five calibrated parameters for adjustment of snow accumulation and melt
	3	T-IED	P-IED	T_S, T_R, *SFCC*, θ, *Kf*	Elevation dependency in the *T* and *P* inputs based on the IED interpolation procedure, and five calibrated parameters for adjustment of snow accumulation and melt
M2	4	T-IDW	P-IDW	*TLR*, *PLR*	Elevation dependency in the *T* and *P* inputs considered based on two calibrated parameters in the SAR, and fixed parameters for snow accumulation and melt
M3	5	T-IDW	P-IDW	*TLR*, *CSV*, *PLR*	Elevation dependency in the *T* and *P* inputs considered based on three calibrated parameters in the SAR, and fixed parameters for snow accumulation and melt
M4	6	T-IDW	P-IDW	*TLR*, *CSV*, *PLR*, θ, *Kf*	Elevation dependency in the *T* and *P* inputs considered based on three calibrated parameters in SAR, and two calibrated parameters for adjustment of snow melt

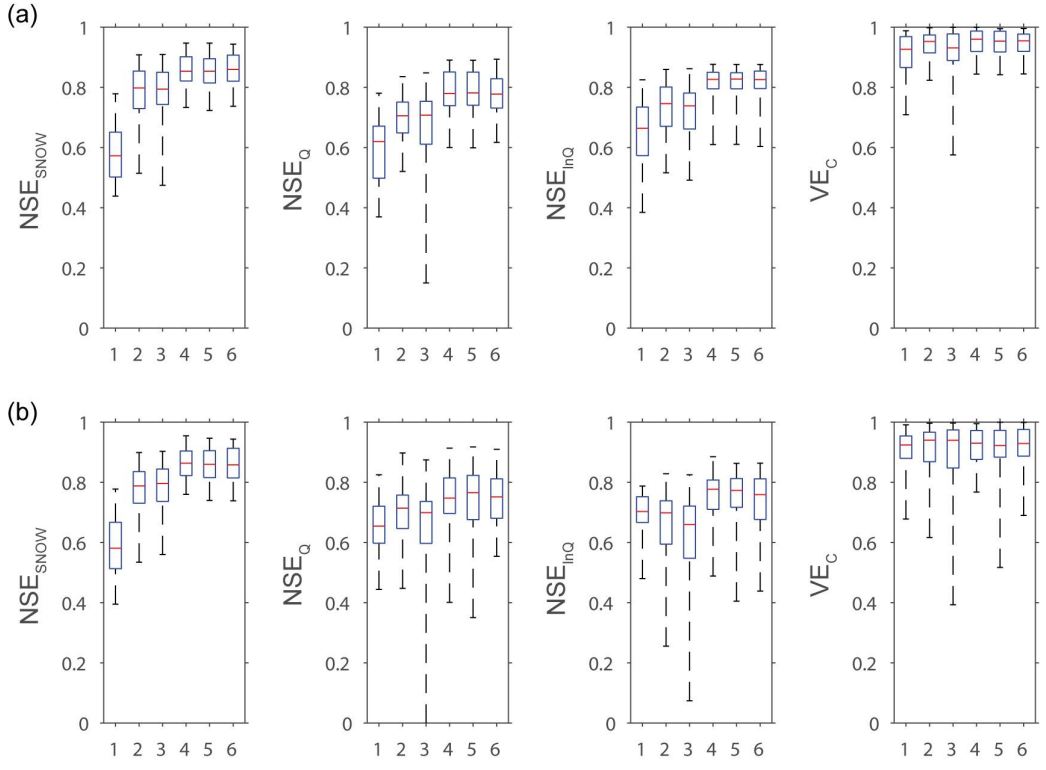

Fig. 5 Boxplots (showing 0.05, 0.25, 0.50, 0.75 and 0.95 percentiles) of the efficiency distributions obtained in validation by the (a) GR4J and (b) HBV9 models combined with the snow model according to six different tests (see Table 5) to account for elevation dependency in the *T* and *P* inputs on the 20 snow-affected Alpine catchments.

https://doi.org/10.5194/hess-2019-556
Preprint. Discussion started: 12 November 2019

Hydrology and Earth System Sciences
Discussions

Figure 5 and Table 6 summarise the efficiency distributions obtained in validation with the GR4J and HBV9 models combined with the snow model in the different tests on the 20 snow-affected Alpine catchments. The results produced by the two hydrological models are in agreement and highlight the following main findings:

- Not considering elevation dependency in either the *T* or *P* inputs (Test #1) leads to notable failures of the snow-hydrological models, due to incorrect snow/rainfall partitioning and snowmelt in space and over time caused by too high temperatures and insufficient input volumes of precipitation, which cannot be offset by the free parameters of the SAR. Notably, calibrating temperature thresholds and ranges for snow/rain partition and snow melt, as well as snow under-catch (using the *SFCC* parameter) is clearly unsatisfactory.
- Considering elevation dependency only in the *T* inputs based on the IED procedure (Test #2) significantly improves the snow-hydrological simulations, but considering elevation dependency in the *P* inputs based on the same procedure (Test #3) is not as efficient, notably for streamflow simulations. This shows that the estimated precipitation with IED over the catchments is of limited accuracy.
- Improving the areal temperature and precipitation estimation clearly requires the calibration of altitudinal temperature and precipitation gradients. The snow-hydrological simulations are considerably improved when using the parsimonious 2-parameter SAR based only on the calibration of *TLR* and *PLR* (Test #4),
- Compared to Test #4 based only on a 2-parameter SAR, only limited improvements in the performance distributions are obtained by introducing additional free parameters to account for the seasonal variability of the temperature gradients (Test #5) and for local adjustment of snowmelt (Test #6).

Table 6 Mean validation efficiency of the 6 modelling tests (see Table 5) on the set of 20 catchments with the GR4J model and the HBV9 model.

Model	Test number	Number of free parameters of the SAR	Mean NSE_{SNOW}	Mean NSE_{Q}	Mean NSE_{lnQ}	Mean VE_{C}
GR4J	1	5	0.59	0.59	0.66	0.91
	2	5	0.79	0.70	0.74	0.94
	3	5	0.79	0.66	0.71	0.90
	4	2	0.86	0.78	0.81	0.95
	5	3	0.86	0.79	0.81	0.95
	6	5	0.86	0.79	0.82	0.95
HBV9	1	5	0.57	0.66	0.70	0.91
	2	5	0.78	0.70	0.67	0.91
	3	5	0.79	0.63	0.61	0.88
	4	2	0.87	0.75	0.74	0.92
	5	3	0.87	0.77	0.76	0.92
	6	5	0.87	0.77	0.76	0.93

Figure 6 shows the differences in the results of the Tests #1 to #4 in terms of annual water balance simulated with the GR4J model in the 20 catchments and represented in a Turc-Budyko non-dimensional space (Le Moine et al., 2007; Valéry et al., 2010; Andréassian and Perrin, 2012). The least stretched and dispersed cluster is obtained when calibrating the altitudinal gradients of temperature and precipitation (Fig. 6d). Compared to the other simulations (Tests #1, #2 and #3), all the dots are located in the narrow "physical" range, delimited by a upper limit where $Q = P$ (i.e., $y = Q/P = 1$) and a lower limit where $Q = P - PE$ ($Q/P = 1 - PE/P \leftrightarrow y = 1 - 1/x$). This means that annual simulated runoff never exceeds total precipitation and that annual runoff deficit never exceeds total *PE* (assuming there are no errors in the streamflow measurements). Altitudinal temperature and precipitation gradients inferred from snow-hydrological modelling thus lead to more realistic catchment water balance than when they are estimated from gauges using interpolation.

As a representative example of the studied catchments, Figure 7 illustrates the differences in the simulations obtained by Tests #1 to #4 for the Durance at Serre-Ponçon. This 3580 km² catchment with altitudes ranging between 652 and 4017 m

https://doi.org/10.5194/hess-2019-556
Preprint. Discussion started: 12 November 2019

Hydrology and Earth System Sciences
Discussions

a.s.l. ensures inflows to one of the biggest dams in Europe (maximum capacity of 1.3 km^3). Dynamics of fractional snow cover area and streamflow are better simulated when considering elevation dependency of the *T* and *P* inputs via two calibrated, altitudinal gradients (Test #4). Compared to the other tests, mean annual temperature (4.1 °C) is lower and mean annual precipitation (1212 mm) is higher. Less precipitation is considered in solid form (44% of total precipitation on average) and accumulation is longer during winter, which fits streamflow observations better, both for low flows from December to April and for flood peaks between May and July. It is worth noting that these more realistic simulations were obtained with a SAR calibrated on only two parameters targeting the local lapse rates whereas the other simulations were based on a SAR calibrated on five parameters. This shows that calibrating the usual snow parameters to compensate for errors in the input data and/or to adapt to local snow processes is less efficient in the simulations than inferring only temperature and precipitation lapse rates while setting all the other parameters to physical or general values. This suggests that adapting to local snow processes is not indispensable and that compensating for the errors in the input data is better achieved by simply calibrating the local temperature and precipitation gradients.

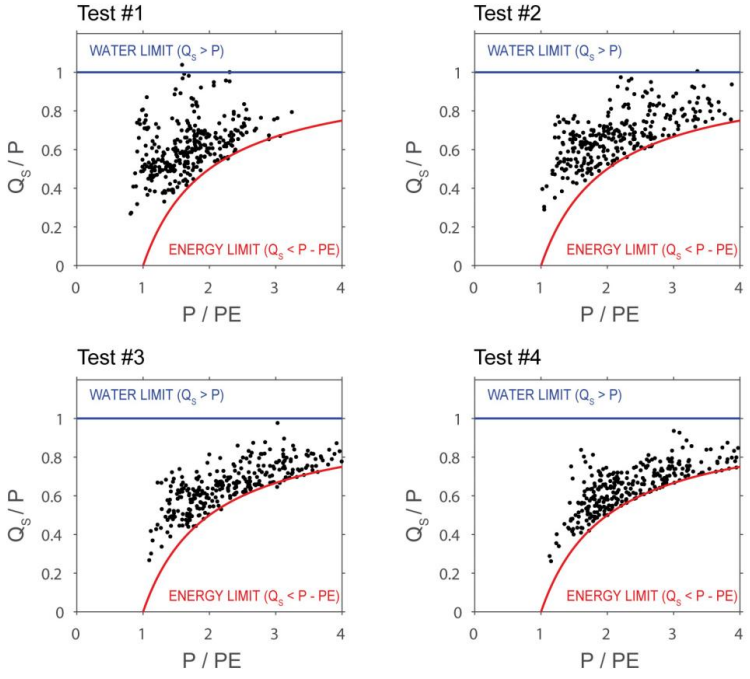

Fig. 6 Simulated annual water balance in validation mapped in non-dimensional space for the 20 snow-affected catchments with the GR4J model according to Tests #1 to #4 (see Table 5). The number of dots is 320, i.e. 20 catchments ×16 years. The Q_S/P versus P/PE plot of Test #4 produces the least stretched and dispersed cluster.

5.3. Identifiability of the parameters

Figure 8 shows an example of parameter sensitivity to the objective function (*OF*) according to the six tests (see Table 5) with the GR4J model on the Durance at Serre-Ponçon. As already shown, considering elevation gradients (Tests #4, #5 and #6) minimises *OF* and improves model performance. It also improves the parameter identifiability. The temperature altitudinal gradient (*TLR*) is easily identifiable with values ranging from 0.66 °C/100 m (Test #4 and Test #5) to 0.70 °C/100m (Test #6). It appears to be a key parameter for improving snow and streamflow simulations compared to parameters calibrated using elevation gradients inferred from interpolation (Tests #2 and #3). The optimum value of the *CSV* parameter (Tests #5 and #6) is zero, clearly indicating no need to account for the seasonal variation in the temperature lapse rate in the

https://doi.org/10.5194/hess-2019-556
Preprint. Discussion started: 12 November 2019

Hydrology and Earth System Sciences
Discussions

catchment studied here. The precipitation lapse rate (*PLR*) is also easy to identify (around 60%/km in the catchment studied). Introducing additional parameters controlling snowmelt (θ and *Kf* in Test #6) does not significantly improve the simulations. This shows that model performance is mainly sensitive to the use of parameters for temperature and precipitation lapse rates and that a 2-parameter SAR based on *TLR* and *PLR* (Test #4) on top of the hydrological models tested is both essential and sufficient to produce satisfactory simulations. Equifinality is more marked for the parameters controlling runoff generation and routing (*X1*, *X2*, *X3* and *X4*), suggesting that these parameters somehow interact. However, the parameter of the inter-catchment groundwater flows (*X2*) shows a clear optimum towards positive values, indicating the need for additional water, which cannot be totally offset by the calibrated precipitation lapse rate. This result suggests that it remains important to explicitly represent inter-catchment groundwater transfers in association with correcting or scaling factors applied to the precipitation input data to render the distribution between evapotranspiration, streamflow and underground fluxes more realistic, as already reported by Le Moine et al. (2007).

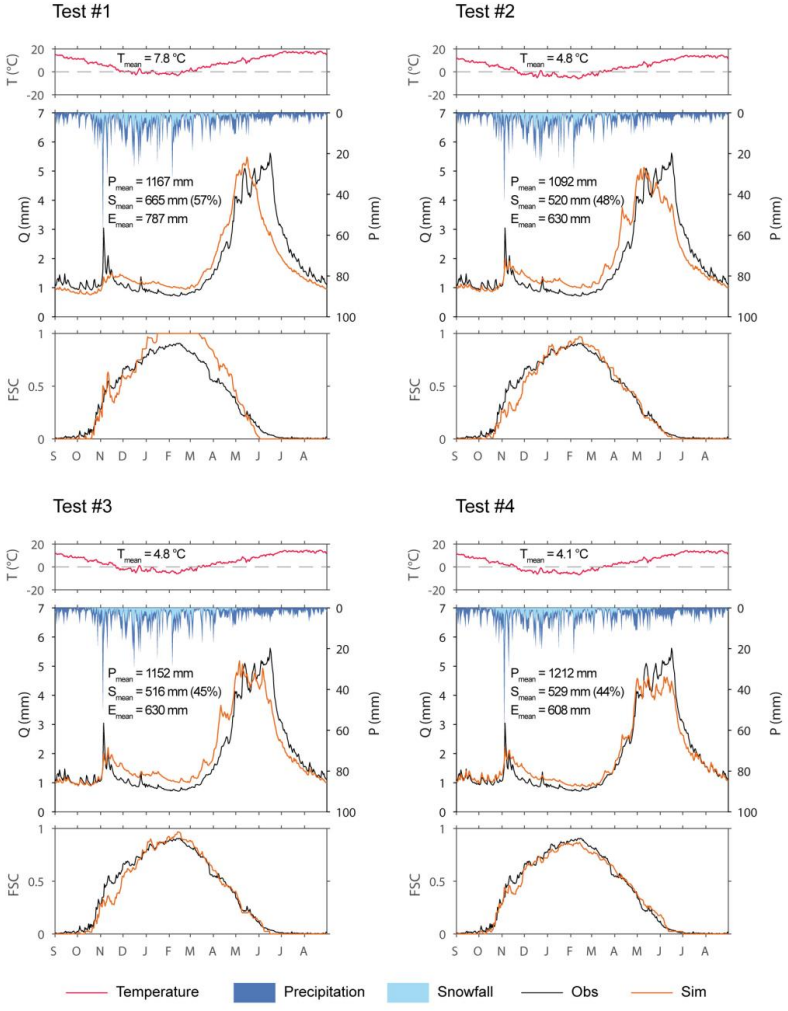

Fig. 7 Comparison of snow-hydrological simulations with elevation dependency according to Tests #1 to #4 (see Table 5) with GR4J for the Durance at Serre-Ponçon. The graphs show mean inter-annual time-series of temperature, precipitation, streamflow and fractional snow cover at the catchment scale in validation over the period 2008–2016. T_{mean}, P_{mean} and S_{mean} stand for mean annual temperature, precipitation, and snowfall, respectively.

https://doi.org/10.5194/hess-2019-556
Preprint. Discussion started: 12 November 2019

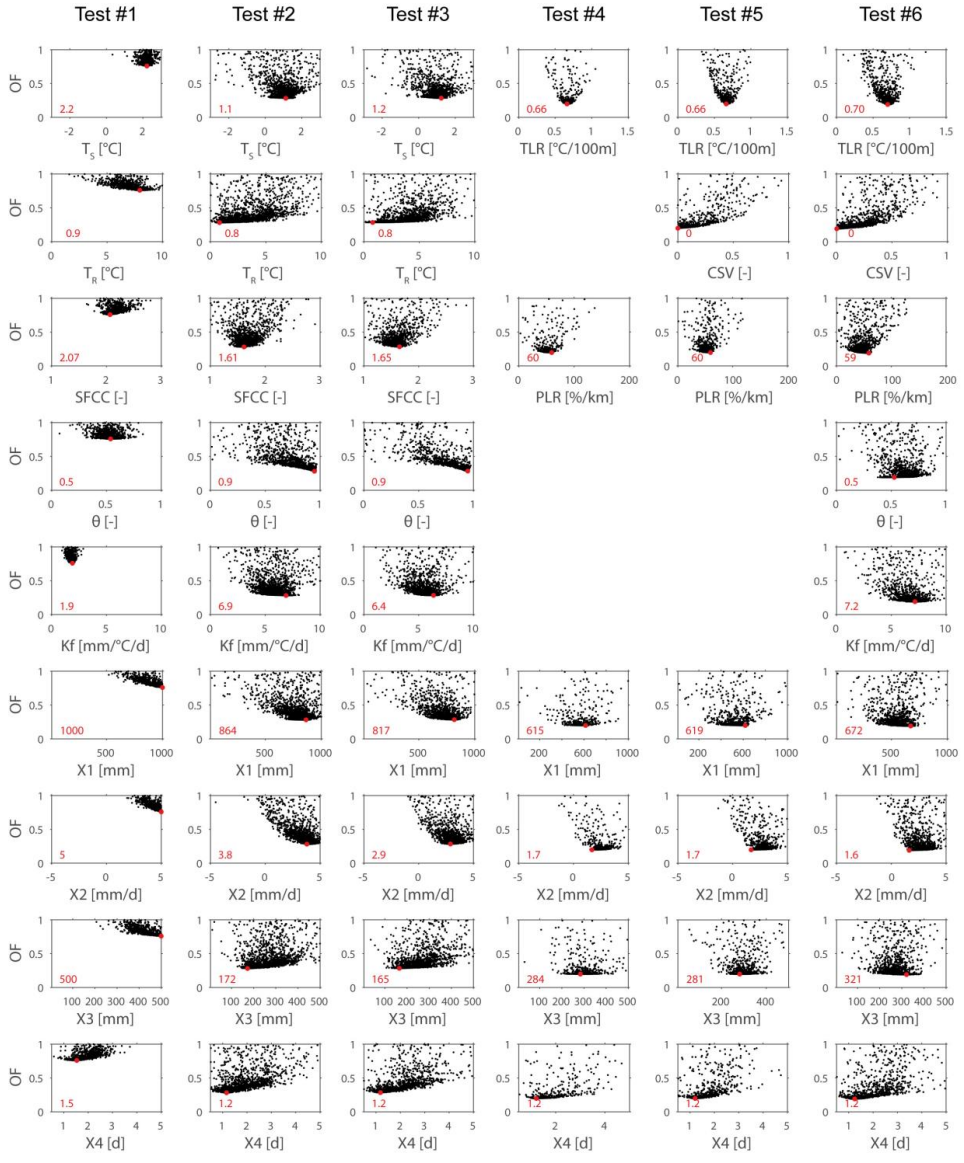

525 **Fig. 8** Parameter sensitivity to the objective function (OF) according to Tests #1 to #6 (see Table 5) with GR4J combined with the snow model on the Durance at Serre-Ponçon. The values and dots in red indicate the optimised calibrated parameters when minimising OF, while the black dots represent trials of the SCE-UA optimisation algorithm.

5.4. Ranges of the calibrated altitudinal gradients

Figure 9 shows that the temperature and precipitation lapse rates vary considerably from one catchment to another.

530 The mean value of the calibrated temperature lapse rates is -0.66 °C (100 m)$^{-1}$ and -0.62 °C (100 m)$^{-1}$ with GR4J and HBV9, respectively. These values are higher than the yearly lapse rates identified by Rolland (2003) from gauge observations in Alpine regions, which ranged from -0.54 to -0.58 °C (100 m)$^{-1}$ in the Italian and Austrian Tyrol. Instead, the values are close to the average temperature gradients generally proposed as approximations in the literature (-0.60 °C in Dodson and Marks, 1997; -0.65 °C (100 m)$^{-1}$ in Barry and Chorley, 1987). They can be used as suitable estimates for daily

https://doi.org/10.5194/hess-2019-556
Preprint. Discussion started: 12 November 2019

Hydrology and Earth System Sciences
Discussions

snow-hydrological purposes in the French Alps. However, to better account for local meteorological conditions, it may be advisable to calibrate them since the *TLR* parameter ranges from -0.43 to -0.84 °C (100 m)$^{-1}$ depending on the catchments and on the models, and is easily identifiable (see Fig. 8 and section 5.3.).

The mean value of the calibrated precipitation lapse rates is 40% (km)$^{-1}$ and 24% (km)$^{-1}$ with GR4J and HBV9, respectively. The differences between the two models may be due to the GR4J ability to gain (or loose) water from inter-catchment groundwater flows through its *X2* parameter (see section 5.3.). On the other hand, HBV9 relies on more parameters for production and transfer, thus enabling to compensate differently for the errors in the precipitation volumes. Whatever the model, the calibrated lapse rates indicate the need for increased precipitation volumes in most catchments, either to counterbalance for erroneous measurements such as the systematic errors associated with precipitation under-catch during snowfall, or to consider the orographic effect that cannot be sufficiently accounted for by the gauges used for interpolating the precipitation fields. However the ranges of the precipitation lapse rates, from 0 to 99% (km)$^{-1}$ with GR4J and from 0 to 79% (km)$^{-1}$ with HBV9, suggest that the required correction is catchment-specific and depends either on the local meteorological conditions or on data from the available surrounding stations to interpolate the daily precipitation.

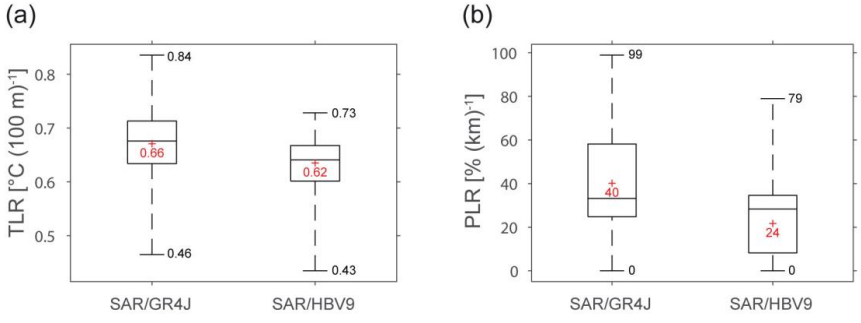

Fig. 9 Boxplots (showing 0.05, 0.25, 0.50, 0.75 and 0.95 percentiles) of the ranges of (a) temperature and (b) precipitation lapse rates calibrated with the 2-parameter SAR (Test #4) in association with the GR4J and HBV9 models on the 20 snow-affected Alpine catchments. The red crosses indicate mean values.

6. SUMMARY AND CONCLUSIONS

6.1. Summary

Elevation is a key factor in spatial climate variability in mountainous areas, for both temperature and precipitation. However, it is still difficult to establish the elevation dependency locally at a daily time scale from scattered observations. The aim of this paper was thus to assess whether snow-covered area and streamflow measurements can help assess altitudinal gradients of temperature and precipitation more realistically than using standard interpolation procedures in data-scarce mountainous areas. To investigate this issue, we used an extensive dataset based on 78 temperature gauges, 148 precipitation gauges, 500-m MODIS gap-filled snow products and 20 streamflow gauges covering the period 2000 to 2016 in the French Alps. Elevation dependency in the temperature and precipitation fields was accounted for using two approaches: (1) by estimating the local and time-varying altitudinal gradients from the available gauge network based on deterministic (inverse distance weighted) and geostatistical (kriging) interpolation methods with external drift; and (2) by calibrating the local gradients using an inverse snow-hydrological modelling framework. In the second approach, we assumed a simple two-parameter correction model to regionalise air temperature and precipitation from the sparse meteorological network: the first parameter (*TLR*) targeted the temperature-elevation relationship, while the second parameter (*PLR*) targeted the precipitation-elevation relationship. The coherence of the two approaches was evaluated by benchmarking several hydrological variables of interest (snow covered area, streamflow and water balance) computed with snow-hydrological models fed by the interpolated

https://doi.org/10.5194/hess-2019-556
Preprint. Discussion started: 12 November 2019

datasets and applied in a modelling framework against available measurements. The advantage of this approach is that it integrates the complex benchmarking process of observational meteorological datasets in an easy-to-grasp metric (Laiti et al., 2018).

Cross-validation of the mapping methods showed that, whatever the time scale, temperature estimates can clearly benefit from taking altitude into account with interpolation methods based on external drift. For precipitation, incorporating elevation in the interpolation methods was especially helpful for yearly and monthly accumulation times but could not achieve an improvement for daily time resolution. Our results also showed that accounting for elevation dependency from gauge networks when interpolating air temperature and precipitation was not sufficient to provide accurate inputs for the snow-hydrological models tested here. The lack of high-elevation stations seriously limited correct estimation of local, time-varying lapse rates of temperature and precipitation, which, in turn, affected the performance of the snow-hydrological simulations due to too imprecise estimates of temperatures and of precipitation volumes. Conversely, retrieving the local altitudinal gradients *via* an inverse modelling approach provided evidence for increased accuracy in the simulation of snow cover and discharge dynamics (including discharge volumes), while limiting the problems of over-calibration and equifinality through parsimonious parametrisation.

6.2. Recommendations

These results suggest that interpolation methods using elevation as external drift such as those tested (KED and IED) should be used with caution in the absence of sufficient high-elevation data. Although the gauge density in the French Alps is close to the minimum density recommended by WMO (2008) for mountainous areas, the number of weather stations is insufficient for a complete cover of the altitude ranges. This seriously limits estimates of local and seasonal relations with elevation, notably for daily precipitation, but also for temperature, which was initially not apparent when using the leave-one-out procedure against available gauges. Placing meteorological fields in a snow-hydrological perspective thus proved indispensable to confirm the limited suitability of standard interpolation methods for generating reliable spatially distributed modelling inputs in mountainous areas. It also made it possible to propose a modelling approach to infer meteorological inputs in complex, mountainous environments and showed that it is possible (and even advisable) to use remotely-sensed snow-cover and streamflow measurements to improve our knowledge of temperature and precipitation inputs in data-scarce mountainous regions. Using auxiliary observations of snow cover notably proved to be useful to give additional insights into the reliability of the modelled snow processes. We thus suggest using the proposed modelling framework to infer local altitudinal gradients from a sparse network of gauges based on key parameters in the snow-hydrological models. More generally, following Tobin et al. (2011), we also recommend using such a framework for a preliminary assessment of the hydrological coherence of gridded datasets to be used in large-scale hydro-climatic studies.

Another recommendation concerns the level of complexity required to control snow accumulation and melt. Most degree-day snow models in the literature use free parameters to adjust snowpack processes and streamflow responses, including the whole water balance. Some parameters (temperature thresholds for snow/rain partition and snowmelt, solid precipitation correction factor) aim to compensate for the errors in the T and P inputs, while others (thermal state of the snowpack, degree-day melt factor) aim to fit snowmelt to local conditions. Our results showed that calibrating these parameters based on a 5-parameter SAR was much less efficient in improving the modelling performance than fixing them and calibrating only local temperature and precipitation altitudinal gradients based on a simple 2-parameter SAR. These results suggest that altitudinal gradients of temperature and precipitation inputs should be inferred from key parameters in snow-hydrological models since they play a first-order role in snow-hydrological simulations. Instead of compensating for the errors in the meteorological inputs, inferring the gradients reduces the input errors originating from the non-representative vertical distribution of stations while allowing the parameters of snow accumulation and melt to be set at

https://doi.org/10.5194/hess-2019-556
Preprint. Discussion started: 12 November 2019

general or physical values. Indeed, introducing additional free parameters to account for the seasonal variability of the temperature gradients and for adjustment of snowmelt led to only limited improvements in the performance distributions compared to the simulations based on the parsimonious 2-parameter SAR. This finding suggests that correcting errors in the model inputs is more critical than adapting the SAR to local snow processes. It also suggests limiting the degree of freedom allowed in degree-day snow models in order to reduce the risk of over-parametrisation.

6.3. Prospects

It would be instructive to further explore the sensitivity of snow-hydrological simulations to seasonal variations in the lapse rates, e.g. by using daily altitudinal gradients instead of a uniform constant gradient. However, as shown in the present paper, establishing the relationship between temperature/precipitation and elevation at the daily time scale from a sparse network of gauges is challenging in mountainous regions. For temperature, the methods tested for computing local and daily lapse rates for each prediction point (KED, IED) outperformed the methods that did not account for altitudinal gradients (IDW, ORK) in the leave-one-out procedure. However, using only a constant lapse rate calibrated from the inverse modelling approach performed substantially better than using the interpolated datasets of temperature with external drift. This shows either that the local temperature lapse rates (including their seasonal variation) were not correctly captured by the daily application of interpolation methods with external drift, or that, for our experiment, accurately estimating a constant, uniform gradient for temperature was more important than estimating its seasonal variations. A seasonal variation in temperature gradient was tested with a sinusoidal approach, which required an additional free parameter to determine the variation interval. When we compared the modified 3-parameter SAR version (Test #5 in Table 5) with the 2-parameter SAR on the whole dataset, we found that the performance distributions of the two SARs were very similar (Fig. 5). This means that, although the seasonal variation in the temperature altitudinal gradient can be put in evidence from gauge networks, as shown by Rolland (2003) for alpine regions, it did not appear indispensable for the daily snow-hydrological processes represented in our modelling experiment. Alternatively, improving the snow-hydrological simulations could consist in using minimum and maximum air temperature rather than daily mean temperature (see e.g. Turcotte et al., 2007) in order to better determine the snow/rain partition. For the regionalisation of these extreme temperatures, one challenge that remains will be characterising the high variability of daily lapse rates, which reflects temperature inversions as well as rapidly changing circulation patterns, as reported in Stahl et al. (2006). The same problem applies to precipitation since the seasonal relationship between precipitation and elevation also depends on exposure to atmospheric flows. Further research could thus build on the works of Jarvis and Stuart (2001) for temperature and Gottardi et al. (2012) for precipitation and focus on methods for interpolation and extrapolation that are capable of accounting for differences in the influence of topography in different seasons and synoptic situations.

Data availability. The hydro-meteorological data and MODIS snow products used in this study are available via the respective websites of the dataset producers: Météo-France (https://publitheque.meteo.fr), Banque Hydro (http://www.hydro.eaufrance.fr), and NASA's National Snow and Ice Data Center (NSIDC, https://nsidc.org) Distributed Active Archive Center (DAAC).

Author contribution. Denis Ruelland conceived the study, performed the analysis and wrote the paper.

Competing interest. The author declares that he has no known competing financial interests or personal relationships that could have appeared to influence the work reported in this paper.

Acknowledgements The author is very grateful to *Météo-France* (https://publitheque.meteo.fr) and *Banque Hydro* (http://www.hydro.eaufrance.fr) for providing the necessary public hydro-meteorological data for the study. NASA's National Snow and Ice Data Center (NSIDC) Distributed Active Archive Center (DAAC) is also acknowledged for providing MODIS snow products (https://nsidc.org), which were used for model calibration and validation.

https://doi.org/10.5194/hess-2019-556
Preprint. Discussion started: 12 November 2019

Hydrology and Earth System Sciences
Discussions

REFERENCES

Ahmed, S., and de Marsily, G.: Comparison of geostatistical methods for estimating transmissivity using data on transmissivity and specific capacity, Water Res. Research, 23, 1717–1737, https://doi.org/10.1029/WR023i009p01717, 1987.

Andréassian, V., and Perrin, C.: On the ambiguous interpretation of the Turc-Budyko nondimensional graph, Water Res. Research, 48, W10601, https://doi.org/10.1029/2012WR012532, 2012.

Bárdossy, A., and Pegram, G.: Interpolation of precipitation under topographic influence at different time scales, Water Res. Research, 49, 4545–4565, https://doi.org/10.1002/wrcr.20307, 2013

Barry, R. G., and Chorley, R. J.: Atmosphere, Weather and Climate. 5th ed. Routledge, 448 pp., 1987.

Beck, H., van Dijk, A. I. J. M., de Roo, A., Miralles, D. G. McVicar, T. R., Schellekens, J., and Bruijnzeel, L. A.: Global-scale regionalization of hydrologic model parameters, Water Res. Research, https://doi.org/10.1002/2015WR018247, 2016.

Bergström, S.: Development of a snow routine for the HBV-2 model, Nordic Hydrol., 6, 73–92, https://doi.org/10.2166/nh.1975.0006, 1975.

Berndt, C., and Haberlandt, U.: Spatial interpolation of climate variables in Northern Germany—Influence of temporal resolution and network density, J. Hydrol. Regional Studies, 15, 184–202, https://doi.org/10.1016/j.ejrh.2018.02.002, 2018.

Deutsch, C. V.: Correcting for negative weights in ordinary kriging, Comput. Geosci., 22, 765–773, https://doi.org/10.1016/0098-3004(96)00005-2, 1996.

Diggle, P. J., and Ribeiro, P. J.: Model-Based Geostatistics, Springer Series in Statistics, Springer, https://doi.org/10.1007/978-0-387-48536-2, 2007.

Dodson, J., and Marks, D.: Daily air temperature interpolated at high spatial resolution over a large mountainous region, Climate Res. 8, 1–20, https://doi.org/10.3354/cr008001, 1997.

Douguédroit, A., and de Saintignon, M. F. : Les gradients de température et de précipitation en montagne, Rev. Geogr. Alp., 72, 225–240, doi :10.3406/rga.1984.2566, 1984.

Drogue, G., Humbert, J., Deraisme, J., Mahr, N., and Freslon, N. : A statistical topographic model using an omnidirectional parameterization of the relief for mapping orographic rainfall, Int. J. Climatol. 22, 599–613, https://doi.org/10.1002/joc.671, 2002.

Duan, Q. Y., Sorooshian, S., and Gupta, V.: Effective and efficient global optimization for conceptual rainfall-runoff models, Water Res. Research, 28, 1015–1031, https://doi.org/10.1029/91WR02985, 1992.

Duan, Q., Sorooshian, S., and Gupta, V.: Optimal use of the SCE-UA global optimization method for calibrating watershed models, J. Hydrol., 158, 265–284. https://doi.org/10.1016/0022-1694(94)90057-4, 1994.

Kuczera, G.: Efficient subspace probabilistic parameter optimization for catchment models, Water Res. Research, 33, 177–185, https://doi.org/10.1029/96WR02671, 1997.

Farr, T. G., Rosen, P. A. , Caro, E., Crippen, R., Duren, R., Hensley, S., Kobrick, M., Paller, M., Rodriguez, E., Roth, L., Seal, D., Shaffer, S., Shimada, J., Umland, J., Werner, M., Oskin, M., Burbank, D., and Alsdorf, D.: The shuttle radar topography mission. Rev. Geophys., 45, RG2004, https://doi.org/10.1029/2005RG000183, 2007.

Franz, K. J., and Karsten, L. R.: Calibration of a distributed snow model using MODIS snow covered area data, J. Hydrol., 494, 160–175, https://doi.org/10.1016/j.jhydrol.2013.04.026, 2013.

Frei, C., and Schär, C.: A precipitation climatology of the Alps from high-resolution rain-gauge observations, Int. J. Climatology, 18, 873–900, https://doi.org/10.1002/(SICI)1097-0088(19980630)18:8<873::AID-JOC255>3.0.CO;2-9, 1998.

Frei, C.: Interpolation of temperature in a mountainous region using nonlinear profiles and non-Euclidean distances, Int. J. Climatolotology, 34, 1585–1605, https://doi.org/10.1002/joc.3786, 2014.

Garavaglia, F., Le Lay, M., Gottardi, F., Garçon, R., Gailhard, J., Paquet, E., and Mathevet, T.: Impact of model structure on flow simulation and hydrological realism from lumped to semi-distributed approach, Hydrol. Earth Syst. Sci., 21, 3937–3952, https://doi.org/10.5194/hess-21-3937-2017, 2017.

https://doi.org/10.5194/hess-2019-556
Preprint. Discussion started: 12 November 2019

Gascoin, S., Hagolle, O., Huc, M., Jarlan, L., Dejoux, J.-F., Szczypta, C., Marti, R., and Sánchez, R.: A snow cover climatology for the Pyrenees from MODIS snow products, Hydrol. Earth Syst. Sci., 19, 2337–2351, https://doi.org/10.5194/hess-19-2337-2015, 2015.

Goovaerts, P.: Geostatistical approaches for incorporating elevation into the spatial interpolation of rainfall, J. Hydrol., 228, 113–129, https://doi.org/10.1016/S0022-1694(00)00144-X., 2000.

Gottardi, F., Obled, C., Gailhard, J., and Paquet, E.: Statistical reanalysis of precipitation fields based on ground network data and weather patterns: Application over French mountains, J. Hydrol., 432–433, 154–167, https://doi.org/10.1016/j.jhydrol.2012.02.014., 2012.

Hall, D., Riggs, G., and Salomonson, V.: MODIS/Terra Snow Cover Daily L3 Global 500m Grid V005, National Snow and Ice Data Center, Boulder, Colorado, USA., 2006.

Hall, D., Riggs, G., and Salomonson, V.: MODIS/Aqua Snow Cover Daily L3 Global 500m Grid V005, National Snow and Ice Data Center, Boulder, Colorado, USA., 2007.

Haylock, M. R., Hofstra, N., Klein Tank, A. M. G., Klok, E. J., Jones, P. D., and New, M.: A European daily high-resolution gridded dataset of surface temperature and precipitation, J. Geophysical Research, 113, D20119, https://doi.org/10.1029/2008JD10201, 2008.

He, Z. H., Parajka, J., Tian, F. Q., and Blöschl, G.: Estimating degree-day factors from MODIS for snowmelt runoff modeling, Hydrol. Earth Syst. Sci., 18, 4773–4789, https://doi.org/10.5194/hess-18-4773-2014, 2014.

Hofstra, N., New, M., and McSweeney, C.: The influence of interpolation and station network density on the distributions and trends of climate variables in gridded daily data, Climate Dynamics, 35, 841–858, https://doi.org/10.1007/s00382-009-0698-1, 2010.

Hublart, P., Ruelland, D., Dezetter, A., and Jourde, H.: Reducing structural uncertainty in conceptual hydrological modeling in the semi-arid Andes, Hydrol. Earth Syst. Sci., 19, 2295–2314, https://doi.org/10.5194/hess-19-2295-2015, 2015.

Hublart, P., Ruelland, D., Garcia de Cortázar-Atauri, I., Gascoin, S., Lhermitte, S., and Ibacache, A.: Reliability of lumped hydrological modelling in a semi-arid mountainous catchment facing water-use changes, Hydrol. Earth Syst. Sci., 20, 3691–3717, https://doi.org/10.5194/hess-20-3691-2016, 2016.

Isotta, F. A., Frei, C., Weilguni, V., Percec Tadic, M., Lassègues, P., Rudolf, B. et al.: The climate of daily precipitation in the Alps: Development and analysis of a high-resolution grid dataset from pan-Alpine rain-gauge data, Int. J. Climatology, 34, 1657–1675, https://doi.org/10.1002/joc.3794, 2014.

Laiti, L., Mallucci, S., Piccolroaz, S., Bellin, A., Zardi, D., Fiori, A., Nikulin, G., and Majone, B.: Testing the hydrological coherence of high-resolution gridded precipitation and temperature data sets, Water Res. Research, 54, https://doi.org/10.1002/2017WR021633, 2018.

Le Moine, N., Andréassian, V., Perrin, C., and Michel, C.: How can rainfall-runoff models handle intercatchment groundwater flows? Theoretical study based on 1040 French catchments, Water Res. Research, 43, W06428, https://doi.org/10.1029/2006WR005608, 2007.

Ly, S., Charles, C., and Degré, A.: Geostatistical interpolation of daily rainfall at catchment scale: the use of several variogram models in the Ourthe and Ambleve catchments, Belgium, Hydrol. Earth Syst. Sci., 15, 2259–2274, https://doi.org/10.5194/hess-15-2259-2011, 2011.

Ly, S., Charles, C., and Degré, A.: Different methods for spatial interpolation of rainfall data for operational hydrology and hydrological modeling at watershed scale: A review, Biotechnol. Agron. Soc. Environ. 17, 392–406, http://hdl.handle.net/2268/136084, 2013.

Masson, D., and Frei, C.: Spatial analysis of precipitation in a high-mountain region: exploring methods with multi-scale topographic predictors and circulation types, Hydrol. Earth Syst. Sci., 18, 4543–4563, https://doi.org/10.5194/hess-18-4543-2014, 2014.

Nash, J. E., and Sutcliffe, J. V.: River flow forecasting through conceptual models – Part I: A discussion of principles, J. Hydrol., 10, 282–290, https://doi.org/10.1016/0022-1694(70)90255-6, 1970.

Nicótina, L., Alessi Celegon, E., Rinaldo, A., and Marani, M.: On the impact of rainfall patterns on the hydrologic response, Water Res. Research, 44, W12401, https://doi.org/10.1029/2007WR006654, 2008.

Oudin, L., Hervieu, F., Michel, C., Perrin, C., Andréassian, V., Anctil, F., and Loumagne, C.: Which potential evapotranspiration input for a lumped rainfall-runoff model? Part 2: towards a simple and efficient potential evapotranspiration model for rainfall-runoff modelling, J. Hydrol., 303, 290–306, https://doi.org/10.1016/j.jhydrol.2004.08.025, 2005.

https://doi.org/10.5194/hess-2019-556
Preprint. Discussion started: 12 November 2019

Oudin, L., Andréassian, V., Mathevet, T., Perrin, C., and Michel, C.: Dynamic averaging of rainfall-runoff model simulations from complementary model parameterizations, Water Res. Research, 42(7), https://doi.org/10.1029/2005WR004636, 2006.

Parajka, J., and Blöschl, G.: The value of MODIS snow cover data in validating and calibrating conceptual hydrologic models, J. Hydrol., 358, 240–258, https://doi.org/10.1016/j.jhydrol.2008.06.006, 2008.

Perrin, C., Michel, C., and Andréassian, V.: Improvement of a parsimonious model for streamflow simulation, J. Hydrol., 279, 275–289, https://doi.org/10.1016/S0022-1694(03)00225-7, 2003.

Rolland, C.: Spatial and seasonal variations of air temperature lapse rates in alpine regions, J. Climate, 16, 1032–1046, https://doi.org/10.1175/1520-0442, 2003.

Sevruk, B.: Regional dependency of precipitation–altitude relationship in the Swiss Alps, Clim. Change 36, 355–369, https://doi.org/10.1023/A:1005302626066, 1997.

Sevruk, B.: Hydrometeorology: rainfall measurement, gauges. In: Anderson, M. G. (Ed.), Encyclopedia of Hydrological Sciences, Vol. 1. Wiley&Sons Ltd., Chichester, UK, pp. 529–535. Ch. 40., 2005.

Shen, S. S. P., Dzikowski, P., Li, G. L., and Griffith, D.: Interpolation of 1961–1997 daily temperature and precipitation data onto Alberta polygons of ecodistrict and soil landscapes of Canada, J. Appl. Meteorol. 40, 2162–2177, https://doi.org/10.1175/1520-0450(2001)040<2162:IODTAP>2.0.CO;2, 2001.

Sinclair, M., Wratt, D., Henderson, R. and Gray, W.: Factors affecting the distribution and spillover of precipitation in the Southern Alps of New Zealand – a case study, J. Appl. Meteorol. 36, 428–442, https://doi.org/10.1175/1520-0450(1997)036<0428:FATDAS>2.0.CO;2, 1997.

Spadavecchia, L., and Williams, M.: Can spatio-temporal geostatistical methods improve high resolution regionalisation of meteorological variables? Agr. Forest Meteorol., 149, 1105–1117, https://doi.org/10.1016/j.agrformet.2009.01.008, 2009.

Stahl, K., Moore, R. D., Floyer, J. A., Asplin, M. G., and McKendry, I. G.: Comparison of approaches for spatial interpolation of daily air temperature in a large region with complex topography and highly variable station density, Agricultural and Forest Meteorology, 139, 224–236, https://doi.org/10.1016/j.agrformet.2006.07.004, 2006.

Thirel, G., Salamon, P., Burek, P., and Kalas, M.: Assimilation of MODIS snow cover area data in a distributed hydrological model using the particle filter, Remote Sens., 5, 5825–5850, https://doi.org/10.3390/rs5115825, 2013.

Tobin, C, Nicótina, L., Parlange, M. B., Berne, A., and Rinaldo, A.: Improved interpolation of meteorological forcings for hydrologic applications in a Swiss Alpine region, J. Hydrol., 401, 77–89, https://doi.org/10.1016/j.jhydrol.2011.02.010, 2011.

Valéry, A., Andréassian, V., and Perrin, C.: Inverting the hydrological cycle: when streamflow measurements help assess altitudinal precipitation gradients in mountain areas. In: New approaches to hydrological prediction in data-sparse regions (Proc. of Symposium HS.2 at the Joint IAHS & IAH Convention, Hyderabad, India, September 2009), IAHS Publ., 333 281–286, 2009.

Valéry, A., Andréassian, V., and Perrin, C.: Regionalization of precipitation and air temperature over high-altitude catchments - learning from outliers, Hydrol. Sci. J., 55, 928–940, https://doi.org/10.1080/02626667.2010.504676, 2010.

Valéry, A., Andréassian, V., and Perrin, C.: As simple as possible but not simpler: What is useful in a temperature-based snow-accounting routine? Part 2 – Sensitivity analysis of the Cemaneige snow accounting routine on 380 catchments, J. Hydrol., 517, 1176–1187, https://doi.org10.1016/j.jhydrol.2014.04.058, 2014.

WMO: Guide to hydrological practices. Volume I: Hydrology – From measurement to hydrological information, 6th edition. World Meteorological Organization, Geneva, 2008.